International Journal of Medical Toxicology & Legal Medicine Volume 27, No. 5, 2024
e-ISSN: 0974-4614
p-ISSN: 0972-0448
https://doi.org/10.47059/ijmtlm/V27I5/125

Topical Delivery of Rifampicin Loaded Lipidic Nanoparticles Gel

Neeraj Kumar[1]*, Rajni Bala[1], Rajeev Ranjan[2]

[1]University School of Pharmaceutical Science Rayat Bahra University Chandigarh
[2]Narayan Institute of Pharmacy Gopal Narayan Singh University Rohtas Bihar
Email: neerajqq9@gmail.com
*Corresponding Author

Received: 21.10.2024 Revised: 17.11.2024 Accepted: 20.12.2024

ABSTRACT

Objective: The objective of the present study was to develop and optimize rifampicin-loaded solid lipid nanoparticles for controlled drug delivery and to evaluate the performance of the optimized formulation.

Methods: Rifampicin-loaded solid lipid nanoparticles were prepared using the hot homogenization followed by ultrasonication method. A Box–Behnken design was applied to optimize lipid concentration, surfactant concentration, and stirring speed. The optimized batch (F2) was evaluated for percentage yield, drug loading, entrapment efficiency, particle size, polydispersity index, zeta potential, in-vitro drug release, FTIR compatibility, and release kinetics.

Results: The optimized formulation F2 exhibited high percentage yield (95.05%), maximum entrapment efficiency (91.25 ± 0.023%), and highest drug loading (9.52 ± 0.12%). Particle size analysis showed a nanosized distribution with a mean particle size of 136.2 nm, low PDI value (0.186), and a high negative zeta potential (−28.4 mV), indicating good stability and uniformity. In-vitro drug release studies revealed sustained release behavior with 99.9 ± 1.45% cumulative drug release over 720 minutes. FTIR analysis confirmed the presence of characteristic functional groups of the drug and excipients without any significant shift, indicating absence of chemical incompatibility. Release kinetic analysis demonstrated that drug release from F2 followed the Higuchi model ($R^2 = 0.8993$), suggesting diffusion-controlled release.

Conclusion: The optimized rifampicin-loaded solid lipid nanoparticle formulation (F2) demonstrated excellent physicochemical characteristics, high drug encapsulation, sustained drug release, and diffusion-controlled release kinetics, indicating its suitability as an effective controlled drug delivery system.

Keywords: Rifampicin; Solid lipid nanoparticles; Optimized formulation; Sustained drug release; Higuchi kinetics

1. INTRODUCTION

Tuberculosis (TB) remains one of the most devastating infectious diseases worldwide, causing significant morbidity and mortality, particularly in low and middle income countries [1]. Despite the availability of effective chemotherapeutic regimens, TB management continues to face major challenges due to prolonged treatment duration, poor patient compliance, systemic toxicity, and the alarming rise of multidrug-resistant tuberculosis (MDR-TB). Conventional oral and parenteral anti-tubercular therapy often results in suboptimal drug concentrations at the site of infection, extensive first-pass metabolism, and dose-related adverse effects, which collectively compromise therapeutic outcomes [2,3].Extrapulmonary and cutaneous forms of tuberculosis, including tuberculous lymphadenitis, lupus vulgaris, and scrofuloderma, present additional therapeutic challenges. Systemic administration of anti-tubercular drugs for localized TB lesions frequently leads to unnecessary systemic exposure while failing to achieve sustained drug levels at the affected site [4]. Therefore, alternative drug delivery strategies capable of localized, controlled, and sustained drug release are highly desirable to enhance treatment efficacy while minimizing systemic toxicity [5,6].

Topical drug delivery offers several advantages for the management of localized tuberculosis infections, including targeted drug action, avoidance of hepatic first-pass metabolism, reduced dosing frequency, and improved patient compliance [7,8,9]. However, effective topical delivery of anti-tubercular drugs is limited by poor skin permeability, inadequate drug retention, and instability of conventional formulations [10]. These limitations necessitate the development of advanced carrier systems capable of enhancing drug penetration and retention within skin layers.Lipid-based nanocarriers, particularly solid lipid nanoparticles (SLNs), have emerged as promising drug delivery systems due to their biocompatibility, biodegradability, ability to encapsulate lipophilic and hydrophilic drugs, and capacity for controlled drug release [11,12,13]. SLNs possess

unique advantages such as nanoscale particle size, large surface area, occlusive properties, and enhanced skin adhesion, making them especially suitable for topical applications [14]. Moreover, SLNs can improve drug stability, enhance permeation through the stratum corneum, and provide sustained drug release at the target site [15,16].In the context of tuberculosis therapy, nanoparticle-based delivery systems have shown potential to improve drug bioavailability, reduce dosing frequency, and enhance intracellular drug uptake by macrophages the primary host cells for *Mycobacterium tuberculosis*[17, 18]. Despite growing interest in nanotechnology-based TB treatment, limited studies have explored the potential of topical lipidic nanoparticle systems for localized anti-tubercular drug delivery [19, 20].

Therefore, the present study aims to develop and optimize anti-tubercular drug-loaded lipidic nanoparticles for topical application. The formulated nanoparticles were characterized for physicochemical properties and evaluated through in-vitro drug release and ex-vivo skin permeation studies to assess their suitability as a localized, effective, and safer therapeutic approach for tuberculosis management [21, 22].

2. MATERIALS AND METHODS

2.1 Materials

Rifampicin was procured from Cipla Pvt. Ltd., India. Glycerol monostearate (GMS), stearic acid, Tween 80, acetone, methanol, and ethanol and potassium dihydrogen phosphate were obtained from Cosmo Chem Pvt. Ltd., India. All chemicals and reagents used in the study were of analytical grade and were used as received without further purification.

2.2 Methods

2.2.1 Evaluation and characterization of solid lipid nanoparticles

Rifampicin loaded SLN were prepared by hot homogenization followed by the ultrasonication method. Rifampicin and stearic acids were dissolved in a mixture of methanol and chloroform (1: 1). Organic solvents were completely removed using a rotary flash evaporator. The embedded lipid layer was melted by heating to 5°C above the melting point of the lipid. An aqueous phase was prepared by dissolving the stabilizers (tween 80 or span 20) in distilled water (sufficient to produce 30 ml) and heating to the same temperature of the oil phase. The hot aqueous phase was added to the oil phase and homogenization was performed (at 2500 rpm and 70°C) using a mechanical stirrer for 30 minutes. The coarse oil in water emulsion so obtained was sonicated using probe sonicator for 25 minutes. Rifampicin loaded SLN was finally obtained by allowing the hot nanoemulsion to cool to room temperature, and was stored at 4°C in the refrigerator [23].

Experimental design

The response surface methodology (RSM) was employed to perform Quality by Design approach for constructing and investigating the polynomial models, using fewer experimental runs. Box-Behnken Design comprising of 3-factors and 3- levels was employed to examine the quadratic response surfaces by assessing the effect of pre-defined independent variables on different response dependent variables Drug Content (%),Entrapment efficiency (%),Drug release (%),Particle size (nm), PDI,Zeta potential and Diffusion rate , was coded as Y1, Y2,Y3,Y4,Y5, Y6 and Y7. Three independent variables namely Lipid conc (%), Surfactant conc (%) and Mechanical stirrer speed (C) were chosen. Each of the variables was varied at two different levels, known as high, and low levels. All the finalized independent variables and the response variables are described in Table 1.

Table 1:List of Independent and Dependent variables in Box–Behnken design

Independent variables	**Lowvalue(-1)**	**Medium value(0)**	**High value(+)**
Lipid conc(%)	5	5.5	6
Surfactant conc(%)	1	1.25	1.5
Stirring speed (rpm)	1000	1500	2000
Dependent variables	Constraints		
Drug Content (%)	Maximize		
Entrapment efficiency (%)	Maximize		
Particle size(nm)	Minimize		

For 30ml

Table 2: DOE suggested and Experimental batches

Formulation code	Rifampicin (mg)	Lipid conc (%)	Stearic acid (gm)	Smixc onc (%)	Total Smixconc(gm)	Surfactant Tween 80 (gm)	Co-surfactant	Stirring speed (RPM)
F1	300	5.5	1.65	1	0.3	0.15	0.15	1000
F2	300	5.5	1.65	1.25	0.375	0.1875	0.1875	1500
F3	300	6	1.8	1.25	0.375	0.1875	0.1875	2000
F4	300	6	1.8	1.5	0.45	0.225	0.225	1500
F5	300	5.5	1.65	1	0.3	0.15	0.15	2000
F6	300	5	1.5	1.25	0.375	0.1875	0.1875	1000
F7	300	5.5	1.65	1.5	0.45	0.225	0.225	2000
F8	300	6	1.8	1.25	0.375	0.1875	0.1875	1000
F9	300	5	1.5	1	0.3	0.15	0.15	1500
F10	300	5	1.5	1.25	0.375	0.1875	0.1875	2000
F11	300	5.5	1.65	1.5	0.45	0.225	0.225	1000
F12	300	6	1.8	1	0.3	0.15	0.15	1500
F13	300	5	1.5	1.5	0.45	0.225	0.225	1500

Smix (surfactant and co-surfactant conc.)

3. EVALUATIONS OF SOLID-LIPID NANOPARTICLE (SLNS)

3.1 Drug Content

The weighed amount of 10 mg formulations powder was taken in a volumetric flask of 10 ml and the volume was made up by methanol and sonicator for 15 min., after that 1 ml of this mixture was diluted to 10 ml by methanol, and the percentage drug content was observed at 337 nm using UV spectrophotometer (Jasco V-630). Calculate drug content by the calibration curve [24].

3.2 Entrapment efficiency (%)

The entrapment efficiency (EE) and drug loading of CS- NPs were determined by separation of NPs from the aqueous medium containing non-associated NPs by centrifugation at 15,000 rpm at 4°C for 45 min (Remi C 25)21. The supernatant was assayed for non-bound drug concentration by UV spectrophotometer (Jasco UV - 630) at 271 nm. The EE (%) of Rifampicin loaded Solid lipid nanoparticles was calculated upon replicating the experiment for three times. The entrapment efficiency, drug loading and practical yields of formulations were calculated from the following equations [25]

$$\text{Enterappedment efficiency (EE\%)} = \frac{\text{Total amount of drug}}{\text{Amount of Entrapped}} \times 100 \ldots\ldots\ldots\ldots 1$$

$$\text{Drug loading (DL\%)} = \frac{\text{Actual drug Content}}{\text{Wieght of obtained product}} \times 100 \ldots\ldots\ldots\ldots\ldots\ldots\ldots\ldots 2$$

3.3 Particle Size, PDI and Zeta potential Analysis

The weighed amount of 10 mg formulations powder was taken and mixed with distilled water and sonication was kept for 30 min. The analysis was performed at a temperature of 25°Csame procedure repeated at zeta potential. The prepared formulations were characterized for zeta- potential in order to know the stability of the formulations[26].

3.4 % yield

To find the percentage yield of solid lipid nanoparticles, the following method was used to compare the mass of the nanoparticles that were made after they were dried gathered and weighed to the mass of the starting materials [27].

$$\text{Pecentage yield} = \frac{\text{Practical yield}}{\text{Theoretical yield}} \times 100$$

3.5 In vitro release Study

The in vitro release of rifampicin from SLN dispersion was determined using the dialysis bag diffusion technique.An accurately weighed amount of rifampicin-loaded Solid lipid nanoparticles containing the drug equivalent to was transfer to a dialysis bag and sealed.The sealed bag was then suspended in a beaker containing 250 ml of phosphate buffer pH 7.4 and stirred at a constant speed of 50 rpm at 37°C ±0.5°C.Aliquots were withdrawn at predetermined intervals from the receptors compartments up to 12 hours and the same was replaced with fresh buffer.Then the drug content was determined spectrophotometrically by measuring the

absorbance 227nm using the phosphate buffer pH7.4 as blank, to calculate the amount of drug release from the nanoparticles [28].

3.6 FTIR spectroscopy

The drug excipients compatibility study was performed by FTIR technique. The Optimized batches F2 samples were scanned over wave number range of 500-4000 cm-1 with diffraction reflectance scanning technique [29].

3.7 Differential Scanning Calorimetry (DSC)

Differential scanning calorimetric (DSC) measurements were carried out on a modulated DSC (Mettler Toledo, SW STARe and USA). The Optimized batch F2 were weighed (2-8mg), the aluminum pans were used and hermetically covered with lead. The heating range was 50-250°C for sample with constant increasing rate of temperature at 10°C /min under nitrogen atmosphere (50-60ml/min). The resultant thermogramof formulation was obtained [30].

3.8 X-ray Diffraction Study

The data obtained from XRD was used to determine whether newly formed compounds are crystalline or amorphous, the following conditions were used for the measurement target metals Cu, filter K, 40kV voltage, and 30 mA current. Optimized batch F2 Samples were scanned over a two-degree range of 10–90°C with a 0.2° phase scale [31].

3.9 Field Emission Scanning Electron Microscopy (FESEM)

Field emission scanning electron microscopy is used to determine the morphology of fractured, surface topography, and texture. The surface morphology of optimized batches F2 was determined by a FESEM (Carl Zeiss, supra55, Germany) at the central instrumental facility (SavitribaiPhule Pune University). Photographs of samples were taken by a different magnification power (200 000x) [32].

4. RESULTS AND DISCUSSION

4.1 Drug Content

Table 3: Drug Content of F1-F13

Formulation code	DrugContent(%)
F1	87.47±0.012
F2	95.26±0.021
F3	90.32±0.052
F4	88.23±0.36
F5	90.09±0.074
F6	85.68±0.089
F7	88.53±0.210
F8	90.06±0.0985
F9	87.76±0.0423
F10	90.64±0.009
F11	85.91±0.001
F12	89.8±0.0810
F13	86.2±0.0341

Conclusion

All formulations showed acceptable drug content (85.68–95.26%). F2 exhibited the highest drug content (95.26%) and was selected as the optimized batch.

ANOVA for Quadratic model

Response1: Drug Content

Drug Content = $95.26 + 1.02A - 0.7813B + 1.31C - 0.0025AB - 1.18AC + 0.0000BC - 3.04A^2 - 4.22B^2 - 3.04C^2$

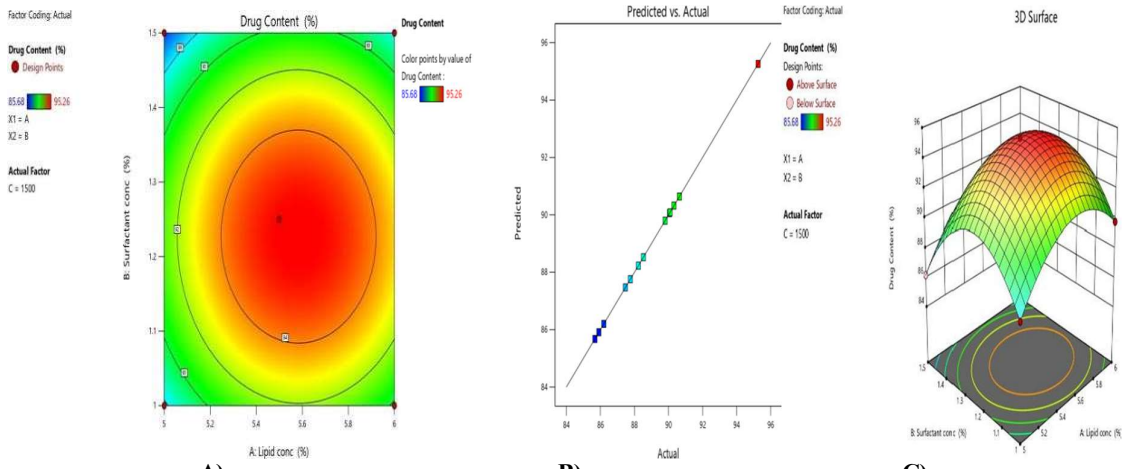

A) **B)** **C)**

Fig. 1A: Counter plot, Figure 2B: Predicted vs. Actual plot, Figure 3C: 3D Surface plot

4.2 Entrapment efficiency (%)

Table 4: Entrapment efficiency of F1-F13

Formulation code	Entrapment efficiency(%)
F1	80.35±0.172
F2	91.25±0.023
F3	85.95±0.0792
F4	84.71±0.051
F5	87.07±0.021
F6	80.45±0.097
F7	82.63±0.041
F8	87.59±0.478
F9	83.74±0.032
F10	88.9±0.0124
F11	85.23±0.001
F12	85.97±0.057
F13	82.74±0.006

Conclusion

Entrapment efficiency of formulations F1–F13 ranged from 80.35% to 91.25%, with F2 showing the highest (91.25%), indicating optimal drug–carrier interaction. Most formulations exhibited high encapsulation (>80%), while F1 and F6 showed comparatively lower efficiency due to suboptimal conditions. F2 was identified as the most promising batch.

ANOVA for Quadratic model

Response 2: Entrapment efficiency

Entrapment efficiency = $91.25 + 1.05A - 0.2275B + 1.37C - 0.0650AB - 2.52AC - 2.33BC - 2.53A^2 - 4.43B^2 - 3.00C^2$

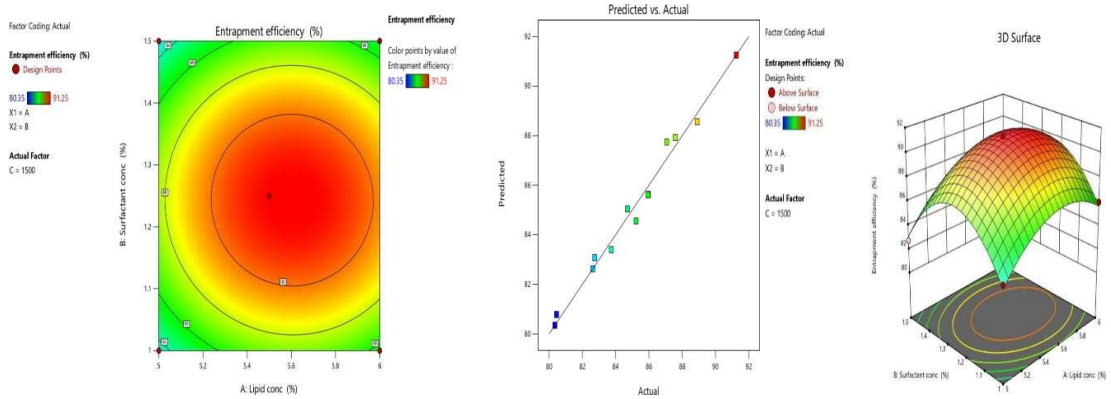

A) B) C)

Fig. 4A: Counter plot, Fig. 5B: Predicted vs Actual plot, Fig. 6C: 3D Surface plot

4.3 Drug Loading

Table 5: Drug Loading of F1-F13

Formulation Code	DrugLoading (%)
F1	8.21 ± 0.18
F2	**9.52 ± 0.12**
F3	7.54 ± 0.21
F4	5.68 ± 0.16
F5	8.41 ± 0.19
F6	7.89 ± 0.14
F7	6.24 ± 0.22
F8	4.56 ± 0.17
F9	8.95 ± 0.15
F10	7.26 ± 0.20
F11	6.25 ± 0.11
F12	7.48 ± 0.18
F13	6.87 ± 0.16

Conclusion

Drug loading of formulations F1–F13 ranged from 4.56% to 9.52%, with F2 showing the highest loading (9.52%), indicating optimal drug incorporation and uniform distribution. Lower loading in F8 and F4 was likely due to suboptimal composition. F2 was identified as the optimized formulation.

4.4 Particle Size, PDI and Zetapotential Analysis

Table 6:Particle Size, PDI and Zetapotential of F1-F13

Formulation Code	Particle size (nm)	PDI	Zeta potential (mV)
F1	184.8	0.263	-22.3
F2	**136.2**	**0.186**	**-28.4**
F3	207.06	0.387	-21.4
F4	222.73	0.214	-20.0
F5	198.62	0.198	-18.4
F6	227.73	0.298	-15.7
F7	147.1	0.191	-23.8
F8	227.08	0.278	-17.6
F9	237.96	0.324	-24.9
F10	204.61	0.362	-27.3
F11	204.07	0.264	-25.7
F12	254.31	0.362	-15.6
F13	237.28	0.412	-13.2

Conclusion

Formulations F1–F13 had nanoscale particle sizes of 136.2–254.31 nm. F2 showed the smallest size (136.2 nm), lowest PDI (0.186), and highest negative zeta potential (−28.4 mV), indicating uniformity and good colloidal stability. Most batches had acceptable homogeneity, while F2 was identified as the optimized formulation.

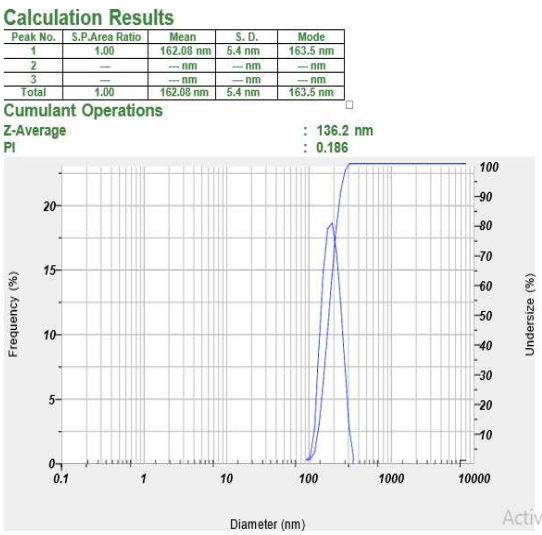

Fig. 7:Particle Size and PDI ofF 2

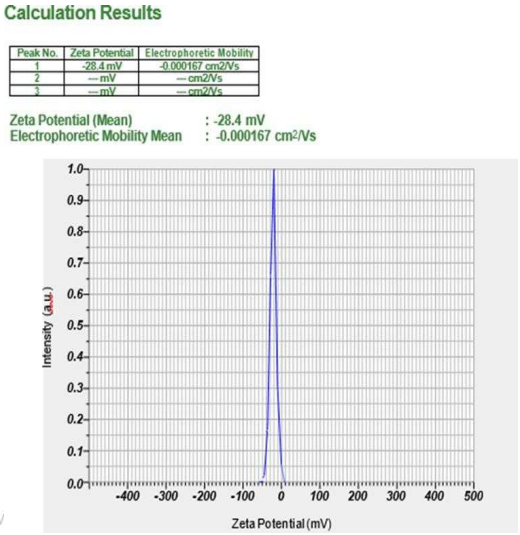

Fig. 8: Zetapotential of F2

Particle size = 136.20 + 0.4500A − 8.06B − 10.79C − 7.72AB + 0.7750AC − 17.70BC + 67.42A² + 34.45B² + 13.00C²

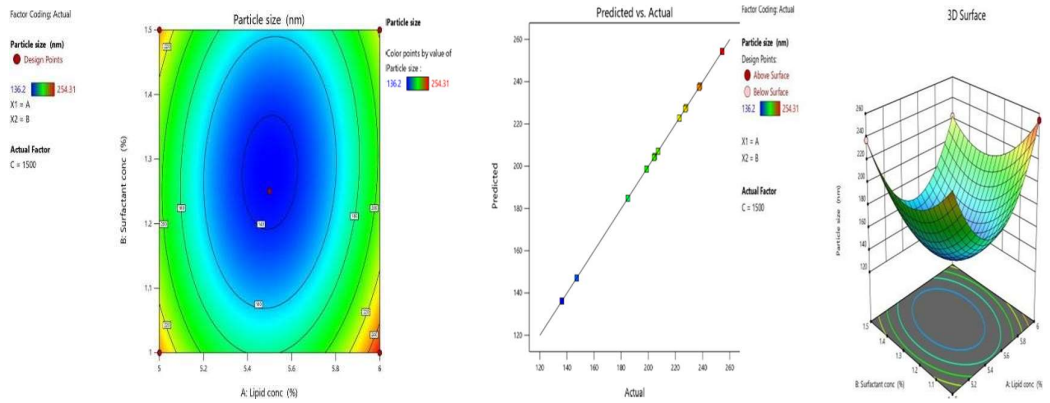

A) B) C)

Fig. 9A: Counter plot, Fig. 10B: Predicted vs Actual plot, Fig. 11C: 3D Surface plot

4.5 %yield

Table 7: % Yield of F1-F13

Formulation Code	TheoreticalYield(mg)	PracticalYield(mg)	%Yield
F1	2250	2020	89.78
F2	**2325**	**2210**	**95.05**
F3	2475	2250	90.91
F4	2550	2280	89.41
F5	2250	2040	90.67
F6	2175	1930	88.74
F7	2400	2140	89.17
F8	2475	2230	90.10
F9	2100	1860	88.57
F10	2175	1960	90.11
F11	2400	2160	90.00
F12	2400	2180	90.83
F13	2250	2010	89.33

Conclusion

The rifampicin formulations (F1–F13) showed percentage yields of 88.57–95.05%. F2 had the highest yield (95.05%), indicating optimal formulation and processing conditions. Overall, the high yields demonstrate good reproducibility, with F2 selected as the optimized batch.

4.6 Invitro release Study

Table 8:Drug release of F1-F6

Time(min)	F1	F2	F3	F4	F5	F6
0	0	0	0	0	0	0
15	8.4 ± 0.32	12.6 ± 0.41	7.9 ± 0.28	6.5 ± 0.24	9.1 ± 0.35	8.0 ± 0.29
30	15.7 ±0.45	21.8 ± 0.52	14.6 ± 0.41	12.3 ± 0.36	16.9 ± 0.48	15.1 ± 0.44
45	24.9 ±0.61	33.5 ± 0.68	23.1 ± 0.59	19.8 ± 0.51	26.4 ± 0.63	24.0 ± 0.57
60	34.8 ±0.73	45.2 ± 0.81	32.7 ± 0.69	27.6 ± 0.62	36.9 ± 0.75	33.1 ± 0.70
90	46.3 ±0.85	58.9 ± 0.92	44.1 ± 0.81	38.2 ± 0.74	49.5 ± 0.88	45.4 ± 0.83
120	55.7 ±0.96	68.4 ± 1.05	53.3 ± 0.92	47.1 ± 0.86	58.6 ± 0.99	54.2 ± 0.94
180	65.8 ±1.08	78.6 ± 1.16	63.5 ± 1.02	56.2 ± 0.95	68.7 ± 1.10	63.9 ± 1.04
240	73.9 ±1.15	85.4 ± 1.22	71.8 ± 1.10	64.1 ± 1.02	76.9 ± 1.18	72.4 ± 1.12
300	80.6 ±1.21	90.3 ± 1.28	78.4 ± 1.17	71.6 ± 1.08	83.2 ± 1.24	78.9 ± 1.19
360	85.4 ±1.26	93.8 ± 1.31	83.1 ± 1.22	77.3 ± 1.15	88.1 ± 1.29	83.5 ± 1.24
420	88.9 ±1.30	96.1 ± 1.35	86.7 ± 1.27	81.9 ± 1.20	91.4 ± 1.33	87.2 ± 1.28
480	91.6 ± 1.33	97.9 ± 1.38	89.8 ± 1.30	85.6 ± 1.24	94.3 ± 1.36	90.1 ± 1.31
540	93.2 ± 1.35	98.6 ± 1.40	91.7 ± 1.33	88.2 ± 1.27	96.1 ± 1.38	92.4 ± 1.34
600	94.6 ± 1.37	99.2 ± 1.42	93.4 ± 1.35	90.1 ± 1.29	97.3 ± 1.40	94.1 ± 1.36
660	95.8 ± 1.39	99.6 ± 1.44	94.7 ± 1.37	91.9 ± 1.31	98.1 ± 1.42	95.5 ± 1.38
720	96.7 ±1.41	99.9 ± 1.45	95.8 ± 1.39	93.4 ± 1.33	98.7 ± 1.44	96.8 ± 1.40

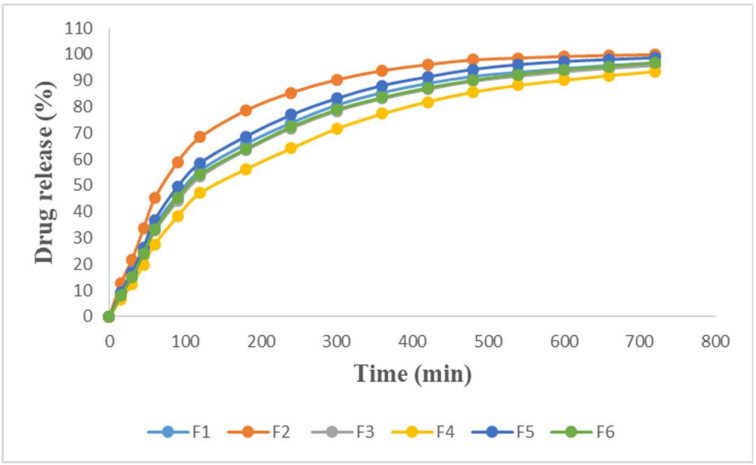

Fig. 12: Drug release of F1-F6

Table 9:Drug release of F7-F13

Time (min)	F7	F8	F9	F10	F11	F12	F13
0	0	0	0	0	0	0	0
15	7.6 ±0.29	6.8 ±0.26	8.4 ±0.31	9.2 ±0.34	7.1 ±0.27	8.0 ±0.30	7.4 ±0.28
30	14.1±0.41	12.8±0.38	15.6 ± 0.44	16.9 ± 0.47	13.5 ± 0.39	14.8 ± 0.42	14.0 ± 0.40
45	22.5 ±0.56	20.4 ±0.52	24.2 ± 0.59	26.1 ± 0.61	21.3 ± 0.54	23.6 ± 0.57	22.7 ± 0.55
60	31.8 ±0.68	28.7 ± 0.64	34.5 ± 0.71	36.9 ± 0.74	30.1 ± 0.66	33.2 ± 0.69	31.6 ± 0.67
90	43.2 ±0.81	39.5 ± 0.77	46.8 ± 0.84	49.6 ± 0.88	41.9 ± 0.79	45.3 ± 0.82	43.7 ± 0.80

120	52.6 ±0.92	48.3 ± 0.88	56.1 ± 0.95	59.2 ± 0.99	51.0 ± 0.90	54.7 ± 0.94	53.1 ± 0.91
180	62.9 ±1.03	58.4 ± 0.98	66.7 ± 1.06	70.1 ± 1.10	61.5 ± 1.01	65.4 ± 1.05	63.8 ± 1.03
240	70.8 ±1.12	66.2 ± 1.07	74.6 ± 1.15	78.2 ± 1.18	69.7 ± 1.10	73.5 ± 1.14	71.9 ± 1.12
300	77.6 ±1.19	72.9 ± 1.14	81.3 ± 1.21	84.7 ± 1.25	76.5 ± 1.17	80.1 ± 1.20	78.8 ± 1.18
360	82.4 ±1.24	77.8 ± 1.19	85.9 ± 1.26	89.1 ± 1.29	81.7 ± 1.22	84.9 ± 1.25	83.6 ± 1.23
420	86.3 ±1.28	81.9 ± 1.23	89.4 ± 1.30	92.3 ± 1.33	85.6 ± 1.26	88.7 ± 1.29	87.2 ± 1.27
480	89.5 ±1.32	85.4 ± 1.27	92.1 ± 1.34	94.8 ± 1.37	88.7 ± 1.30	91.5 ± 1.33	90.1 ± 1.31
540	91.8 ±1.35	88.1 ± 1.30	94.3 ± 1.37	96.6 ± 1.40	90.9 ± 1.33	93.7 ± 1.36	92.4 ± 1.34
600	93.6 ±1.37	90.4 ± 1.33	96.1 ± 1.39	98.1 ± 1.42	92.7 ± 1.36	95.4 ± 1.38	94.0 ± 1.36
660	95.1 ±1.39	92.3 ± 1.35	97.4 ± 1.41	99.0 ± 1.44	94.1 ± 1.38	96.8 ± 1.40	95.5 ± 1.38
720	96.4 ±1.41	93.9 ± 1.37	98.3 ± 1.43	99.6 ± 1.46	95.3 ± 1.40	97.9 ± 1.42	96.8 ± 1.41

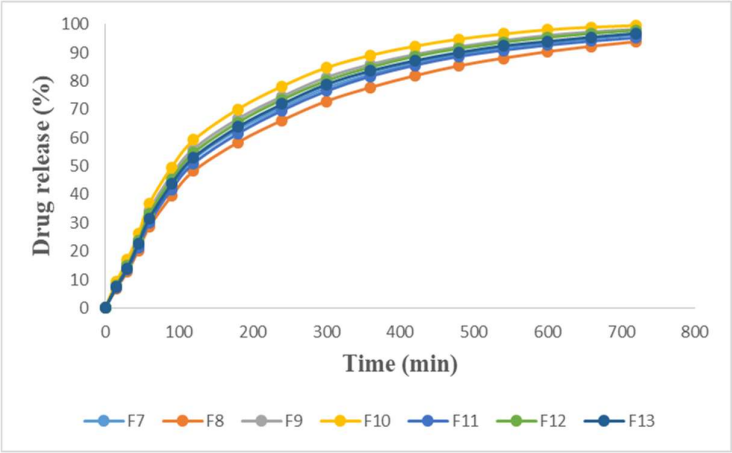

Fig. 13: Drug release of F7-F13

Conclusion

Formulations F1–F13 showed sustained, time-dependent drug release over 720 minutes. F2 exhibited the highest release (99.9 ± 1.45%), while F10 showed the maximum among F7–F13 (99.6 ± 1.46%). Low variability indicates uniform drug distribution. F2 and F10 were identified as the most promising formulations for controlled release.

Kinetic analysis of drug release-

The in vitro release data of the optimized batch (F2) were fitted to kinetic models—zero-order, first-order, and Higuchi—to determine the release mechanism. The rate constants (k) and determination coefficients (R^2) were calculated to identify the model that best describes the release pattern.

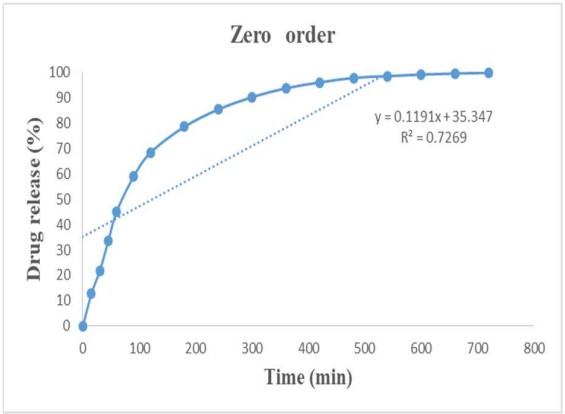

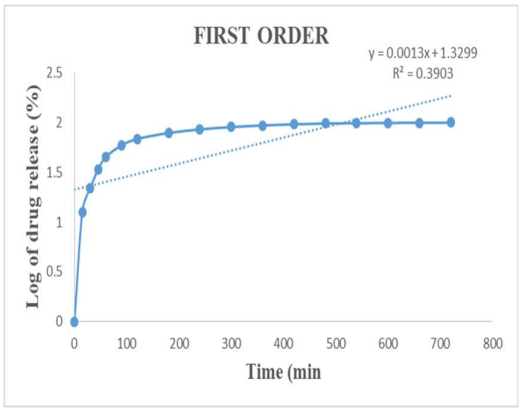

Fig. 14: Zero order model of F2Figure 15: First order

Table 10:ZERO ORDER MODEL

ZERO ORDER MODEL	
Formulation Code	**R2Value**
F2	0.7269

Table 11: FIRST ORDER MODEL

FIRST ORDER MODEL	
Formulation Code	**R2 Value**
F2	0.3903

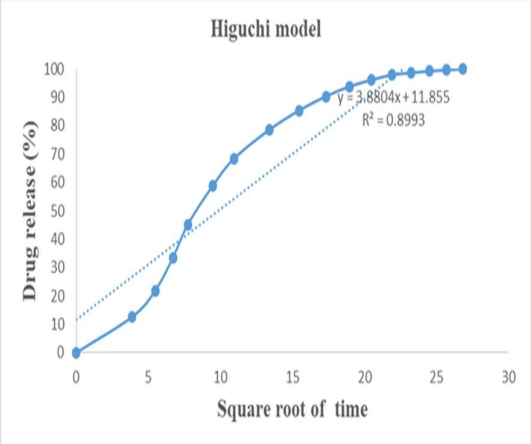

Fig.16:Higuchi model of F2

HIGUCHIMODEL	
FormulationCode	**R2Value**
F2	0.8993

Table 12: HIGUCHI MODEL

Conclusion

The in vitro release data of formulation F2 were fitted to zero-order, first-order, and Higuchi models to determine the release mechanism. The Higuchi model showed the highest correlation (R^2 = 0.8993), indicating that drug release from F2 is predominantly governed by diffusion through the polymeric matrix, while zero-order (R^2 = 0.7269) and first-order (R^2 = 0.3903) models were less representative.

4.7 FTIR spectroscopy

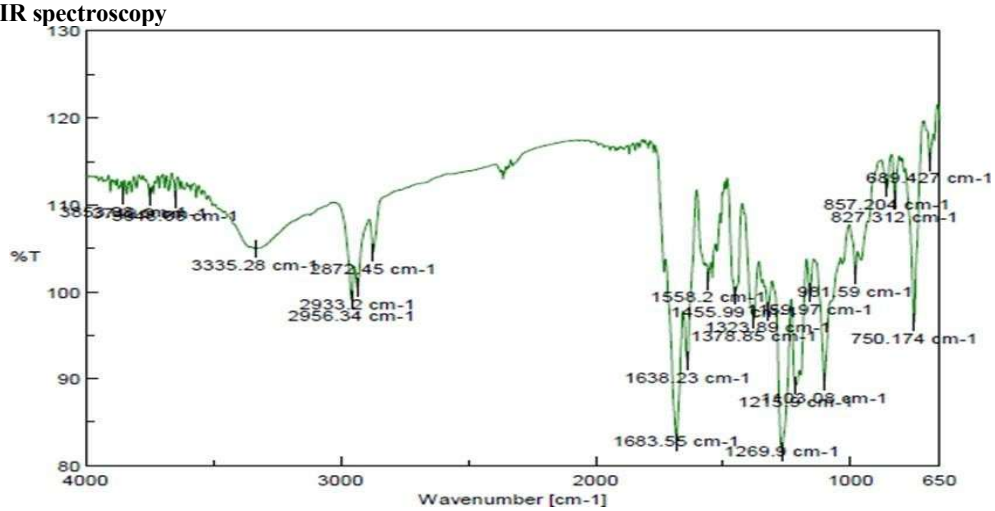

Fig. 17: FTIR Spectrum of F2

Conclusion

FTIR of formulation F2 confirmed successful incorporation of the drug into the matrix, with all characteristic functional groups of the drug and excipients preserved. Key peaks included O–H stretching (3335 cm^{-1}), aliphatic C–H stretching (2956, 2933 cm^{-1}), C=O stretching (1683 cm^{-1}), aromatic C=C (1638 cm^{-1}), amide II (1558 cm^{-1}), C–H bending and C–N stretching (1456, 1379 cm^{-1}), C–O and C–O–C stretching (1269, 1215, 1159 cm^{-1}), and aromatic C–H bending (981–699 cm^{-1}). No significant shifts or new peaks were observed, indicating no chemical interaction or incompatibility between the drug and excipients.

4.8 Differential Scanning Calorimetry (DSC)

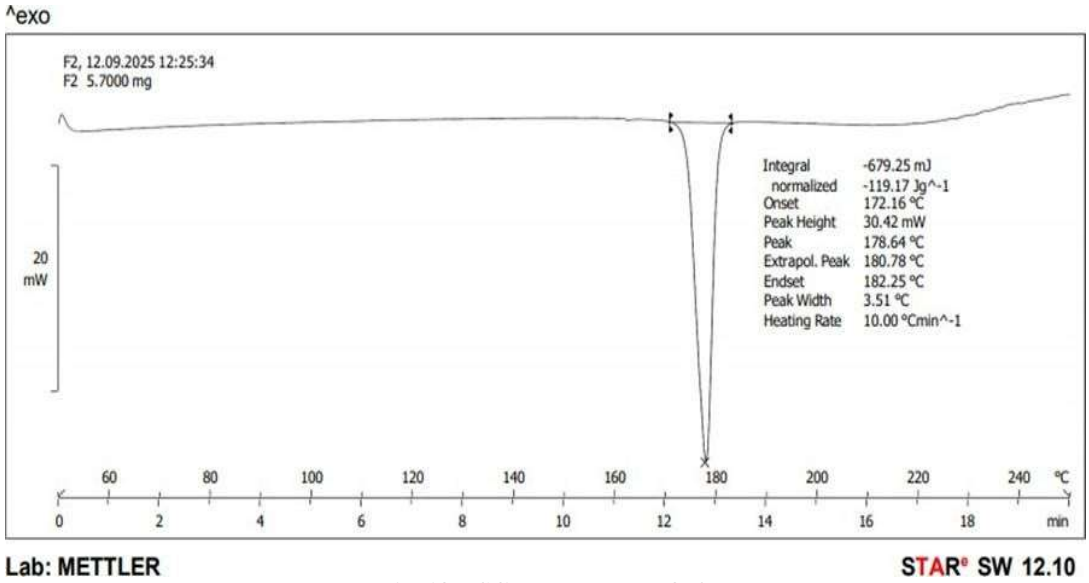

Fig. 18:DSC thermogram of F2

Conclusion

The DSC shows a sharp endothermic peak at 178.64 °C, indicating drug melting with good thermal stability. The slight shift suggests drug–excipient interaction without degradation, confirming successful formulation.

4.9 X-ray Diffraction Study

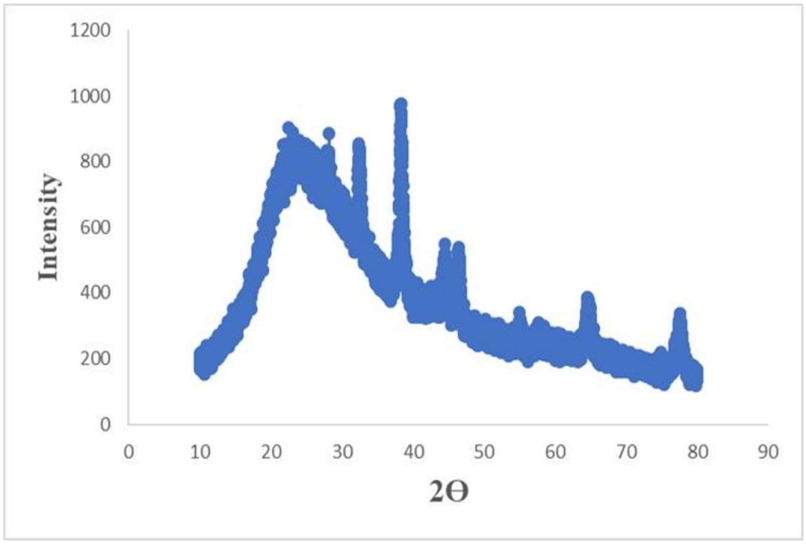

Fig. 19: X-ray Diffract gram of F2

Conclusion

The X-ray Diffractogram of F2 exhibits a broad halo pattern without sharp, well-defined peaks, confirming that the peak is amorphous in nature. This indicates loss of crystalline structure of the drug in the formulation, suggesting successful incorporation into the polymer matrix, which is advantageous for improved solubility and controlled drug release.

4.10 Field Emission Scanning Electron Microscopy (FESEM)

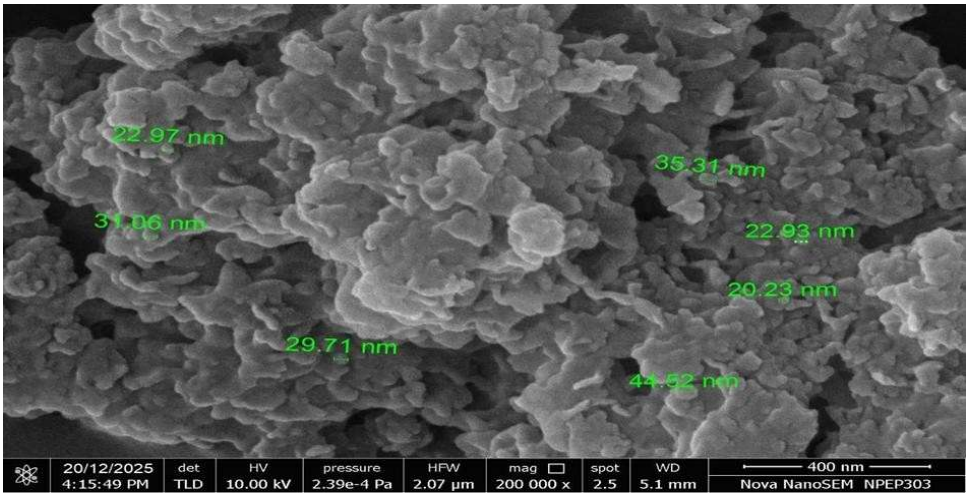

Fig.20: Field Emission Scanning Electron Microscopy of F2

Conclusion

Field Emission Scanning Electron Microscopy (FESEM) of F2 reveals irregular, clustered nanoparticles with a rough and porous surface morphology. The particles are predominantly in the nanoscale range (~20–45 nm), indicating successful nanosizing. Slight agglomeration is observed, which is common for amorphous nanoparticulate systems due to high surface energy.Overall, the morphology supports uniform particle formation and is favorable for enhanced surface area and drug release performance.

5. SUMMARY

The present study focused on the development and optimization of rifampicin-loaded solid lipid nanoparticles (SLNs) for topical delivery using a Quality by Design approach. SLNs were prepared by hot homogenization followed by ultrasonication and optimized using a Box–Behnken design by varying lipid concentration, surfactant concentration, and stirring speed. Thirteen formulations (F1–F13) were prepared and evaluated for drug content, entrapment efficiency, drug loading, particle size, PDI, zeta potential, percentage yield, and in-vitro drug release. Formulation F2 consistently showed superior performance with the highest drug content (95.26%), maximum entrapment efficiency (91.25%), highest drug loading (9.52%), smallest particle size (136.2 nm), lowest PDI (0.186), highest negative zeta potential (−28.4 mV), and maximum percentage yield (95.05%). In-vitro drug release studies demonstrated sustained release over 720 minutes, with F2 showing the highest cumulative release (99.9%). Release kinetics of F2 best fitted the Higuchi model (R^2 = 0.8993), indicating diffusion-controlled drug release. FTIR, DSC, XRD, and FESEM analyses confirmed successful drug incorporation, absence of chemical incompatibility, amorphous nature of the drug, and suitable nanoparticle morphology.

6. CONCLUSION

Rifampicin-loaded solid lipid nanoparticles were successfully developed and optimized using response surface methodology. Among all formulations, F2 was identified as the optimized batch based on superior drug content, entrapment efficiency, drug loading, nanoscale particle size, good stability, high percentage yield, and sustained drug release behavior. Kinetic modeling confirmed diffusion-controlled release following the Higuchi model. FTIR, DSC, XRD, and FESEM studies demonstrated compatibility between drug and excipients, thermal stability, amorphization of the drug, and favorable nanoparticle morphology. Overall, the developed rifampicin-loaded SLN system shows promise as a controlled and effective topical delivery system for tuberculosis management.

REFERENCE

1. World Health Organization. WHO consolidated guidelines on tuberculosis. Module 2: screening-systematic screening for tuberculosis disease. World Health Organization; 2021 Mar 22.
2. Zhang Y, Shi W, Zhang W, Mitchison D. Mechanisms of pyrazinamide action and resistance. Microbiology spectrum. 2014 Aug 30;2(4):10-128.
3. Bozdogan B, Appelbaum PC. Oxazolidinones: activity, mode of action, and mechanism of resistance. International journal of antimicrobial agents. 2004 Feb 1;23(2):113-9.
4. Singhvi G, Girdhar V, Patil S, Gupta G, Hansbro PM, Dua K. Microbiome as therapeutics in vesicular delivery. Biomedicine & Pharmacotherapy. 2018 Aug 1; 104:738-41.

5. Patil K, Bagade S, Bonde S, Sharma S, Saraogi G. Recent therapeutic approaches for the management of tuberculosis: Challenges and opportunities. Biomedicine & pharmacotherapy. 2018 Mar 1; 99:735-45.
6. Canetti G, Fox W, Khomenko AA, Mahler HT, Menon NK, Mitchison DA, Rist N, Šmelev NA. Advances in techniques of testing mycobacterial drug sensitivity, and the use of sensitivity tests in tuberculosis control programmes. Bulletin of the World Health Organization. 1969;41(1):21.
7. Zhang Y. Genetic basis of isoniazid resistance of Mycobacterium tuberculosis. Research in microbiology. 1993 Jan 1;144(2):143-9.
8. Ferrazoli L, Palaci M, da Silva Telles MA, Ueki SY, Kritski A, Marques LR, Ferreira OC, Riley LW. Catalase expression, katG, and MIC of isoniazid for Mycobacterium tuberculosis isolates from Sao Paulo, Brazil. Journal of Infectious Diseases. 1995 Jan 1;171(1):237-40.
9. Silva MS, Senna SG, Ribeiro MO, Valim AR, Telles MA, Kritski A, Morlock GP, Cooksey RC, Zaha A, Rossetti ML. Mutations in katG, inhA, and ahpC genes of Brazilian isoniazid-resistant isolates of Mycobacterium tuberculosis. Journal of clinical microbiology. 2003 Sep;41(9):4471-4.
10. Jaber M, Rattan A, Kumar R. Presence of katG gene in resistant Mycobacterium tuberculosis. Journal of clinical pathology. 1996 Nov 1;49(11):945-7.
11. Carvalho WS, Spindola de Miranda S, Costa KM, Araújo JG, Augusto CJ, Pesquero JB, Pesquero JL, Gomes MA. Low-stringency single-specific-primer PCR as a tool for detection of mutations in the rpoB gene of rifampin-resistant Mycobacterium tuberculosis. Journal of Clinical Microbiology. 2003 Jul;41(7):3384-6.
12. Houben RM, Dodd PJ. The global burden of latent tuberculosis infection: a re-estimation using mathematical modelling. PLoS medicine. 2016 Oct 25; 13(10):e1002152.
13. Jayasankar K, Ramanathan VD. Biochemical &histochemical changes relating to fibrosis following, infection with Mycobacterium tuberculosis in the guineapig. Indian Journal of Medical Research. 1999;110(Sep):91-7.
14. Cohn ZA. The fate of bacteria within phagocytic cells: I. The degradation of isotopicallylabeled bacteria by polymorphonuclear leucocytes and macrophages. The Journal of experimental medicine. 1963 Jan 1;117(1):27-42.
15. Walker L, Lowrie DB. Killing of Mycobacterium microti by immunologically activated macrophages. Nature. 1981 Sep 3;293(5827):69-70.
16. Chan J, Flynn J. Nitric oxide in Mycobacterium tuberculosis infection. InNitric oxide and Infection 1999 Jul 31 (pp. 281-307). Boston, MA: Springer US.
17. Rook GA, Steele J, Ainsworth M, Champion BR. Activation of macrophages to inhibit proliferation of Mycobacterium tuberculosis: comparison of the effects of recombinant gamma-interferon on human monocytes and murine peritoneal macrophages. Immunology. 1986 Nov;59(3):333.
18. World Health Organization. Guidelines for surveillance of drug resistance in tuberculosis. World Health Organization; 2009.
19. Koh WJ, Ko Y, Kim CK, Park KS, Lee NY. Rapid diagnosis of tuberculosis and multidrug resistance using a MGIT 960 system. Annals of laboratory medicine. 2012 Jun 20;32(4):264.
20. World Health Organization. The use of molecular line probe assays for the detection of resistance to isoniazid and rifampicin. InThe use of molecular line probe assays for the detection of resistance to isoniazid and rifampicin 2016.
21. Katale BZ, Mbelele PM, Lema NA, Campino S, Mshana SE, Rweyemamu MM, Phelan JE, Keyyu JD, Majigo M, Mbugi EV, Dockrell HM. Whole genome sequencing of Mycobacterium tuberculosis isolates and clinical outcomes of patients treated for multidrug-resistant tuberculosis in Tanzania. BMC genomics. 2020 Feb 21;21(1):174.
22. Nahid P, Mase SR, Migliori GB, Sotgiu G, Bothamley GH, Brozek JL, Cattamanchi A, Cegielski JP, Chen L, Daley CL, Dalton TL. Treatment of drug-resistant tuberculosis. An official ATS/CDC/ERS/IDSA clinical practice guideline. American journal of respiratory and critical care medicine. 2019 Nov 15;200(10):e93-142.
23. Ekambaram P, Sathali AA. Formulation and evaluation of solid lipid nanoparticles of ramipril. Journal of young pharmacists. 2011 Jul 1;3(3):216-20.
24. De Gaetano F, Cristiano MC, Venuti V, Crupi V, Majolino D, Paladini G, Acri G, Testagrossa B, Irrera A, Paolino D, Tommasini S. Rutin-loaded solid lipid nanoparticles: characterization and in vitro evaluation. Molecules. 2021 Feb 16;26(4):1039.
25. Rukmangathen R, Yallamalli IM, Yalavarthi PR. Formulation and biopharmaceutical evaluation of risperidone-loaded chitosan nanoparticles for intranasal delivery. Drug Development and Industrial Pharmacy. 2019 Aug 3;45(8):1342-50.
26. Mohammad A, Ghareeb M. Tacrolimus monohydrate loaded lipid polymer hybrid nanoparticles Formulation and stability study. Kerbala J Pharm Sci. 2021;1:19.
27. Patel S, Chavhan S, Soni H, Babbar AK, Mathur R, Mishra AK, Sawant K. Brain targeting of risperidone-

loaded solid lipid nanoparticles by intranasal route. Journal of drug targeting. 2011 Jul 1;19(6):468-74.
28. Chandana M, Ramana MV, Rao NR. Formulation and evaluation of Valsartan solid lipid nanoparticles. J Drug DelivTher. 2021;11(2-S):103-8.
29. Shah P, Chavda K, Vyas B, Patel S. Formulation development of linagliptin solid lipid nanoparticles for oral bioavailability enhancement: role of P-gp inhibition. Drug delivery and translational research. 2021 Jun;11(3):1166-85.
30. Gardouh AR, Gad S, Ghonaim HM, Ghorab MM. Design and characterization of glycerylmonostearate solid lipid nanoparticles prepared by high shear homogenization. British journal of pharmaceutical research. 2013 Jul 1;3(3):326.
31. Musielak E, Feliczak-Guzik A, Nowak I. Optimization of the conditions of solid lipid nanoparticles (SLN) synthesis. Molecules. 2022 Mar 28; 27(7):2202.
32. Imran U, Aundhia C, Seth A, Chauhan S, Shah N. Formulation and Evaluation of Solid lipid nanoparticles: Isoniazid. PharmaTutor. 2014 Oct 1;2(10):129-35.